UNSTEADY WALL PRESSURE FIELD OF A MODEL A-PILLAR CONICAL VORTEX

Cédric Hoarau, Jacques Borée, Janick Laumonier, Yves Gervais
Laboratoire d'Etudes Aérodynamiques,
Université de Poitiers, ENSMA, CNRS
Téléport 2 ; 1, avenue Clément Ader BP 40109
86961 Futuroscope Chasseneuil, France
jacques.boree@lea.ensma.fr

ABSTRACT

The spatio-temporal properties of the unsteady wall pressure field of a model A-pillar conical vortex are studied in this paper by combining 2 components LDV measurements and multi-points pressure measurements using off-set microphones. Detailed LDV measurements are displayed and discussed in the vortex region. A spectral analysis of the fluctuating pressure under the vortex core is used to analyse the link between the temporal and spatial scales of the unsteady aerodynamic and the wall pressure field. We show that the conical vortex is a guide for the velocity perturbations and that their hydrodynamic pressure footprint is transported at the measured mean axial velocity in a local reference frame aligned with the vortex core. The energy containing higher frequency parts of the PSD are only weakly correlated when distant sensors are considered. However, two distinct peaks of coherence at lower frequencies are observed and discussed physically. The distinct contributions extracted here have a significant impact as Cp' is concerned and should be transmitted in very different ways by the car structure because the frequency and length scale range is very distinct.

1- INTRODUCTION

Conical vortices generated over surfaces having a swept angle with the incident wind are important features for civil engineering (Kawai and Nishimura 1996) and transport engineering. The study presented here has a strong link with the aerodynamic and aero-acoustic of passenger vehicles. More particularly, we focus on the study of a model A-pillar conical vortex. Previous studies (See Alam, Watkins et al. (2003) and references therein) have clearly established that the flow around a passenger car's A-pillar region is a major source of "in-cabin" aerodynamic noise. The main source is due to the resultant fluctuating pressure on the vehicle structure. Of course, large A-pillar radii and avoidance of flow separation can be very efficient to minimize the aerodynamic noise. Unfortunately, such constraints can be in conflict with style constraints. There is therefore a need for analysis, even in model situations with sharp edges, with the hope of finding efficient control strategies that would be efficient whatever the geometry. An important particularity of these A-pillar structures is their strong interaction with the lateral wall of the car. This differs from delta wing leading edge vortices at high angle of attack (Delery 1994). The paper of (Alam, Watkins et al. 2003) presents a very interesting parametric study of the mean and fluctuating pressure measurements for a family of idealized road vehicles at different yaw angles. Unfortunately, no measurements of the associated velocity field were provided. The maximum fluctuating pressure coefficient is large for slanted sharp-edge A-pillar (≈ 30% at 0° yaw angle) and located under the separated conical vortex. Power spectral densities were also presented and preferential Strouhal numbers were identified. However, these Strouhal numbers are based on an arbitrarily chosen length scale and are therefore difficult to associate with particular physical events. This observation motivates the use of multi-point analyzing techniques.

Our objectives in the present work were the following: (i) to present a model geometry that can be used for physical analysis and further control studies (Lehugeur and Gillieron 2006) ; (ii) to provide a measurement of the mean and fluctuating velocity field in the conical vortex region ; (iii) to provide multi-points simultaneous measurements of the surface pressure in order to be able to understand the spatio-temporal evolution of the fluctuating wall pressure.

The experimental set-up and measurements techniques are presented next. Mean and fluctuating velocity fields in the conical vortex and spatio-temporal properties of the fluctuating pressure at the wall are then discussed. A physical discussion is proposed in section 4. The link between both sets of measurements, when using for the velocity a local referential aligned with the core of the vortex, is believed to highlight clearly the mean transport of the large scale perturbations in the conical vortex and the associated length scales

2 - EXPERIMENTAL SET-UP AND MEASUREMENTS TECHNIQUES

A picture of the body is shown in figure 1. The length and width of the base surface are L=400 mm and W=120 mm. The height of the model is H=90 mm. The two lateral sides

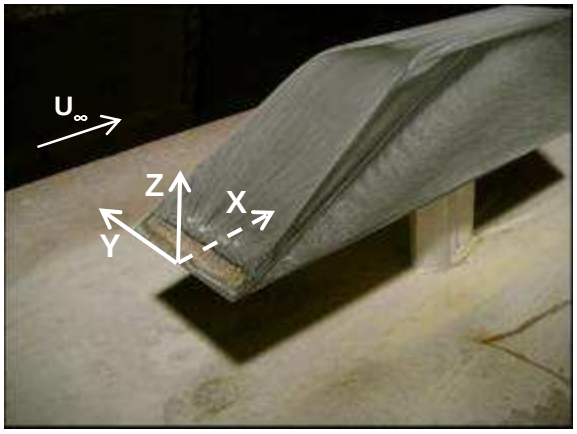

Figure 1 : Picture of the body. Oil flow visualisation obtained with a mixture of white spirit and kaolin powder

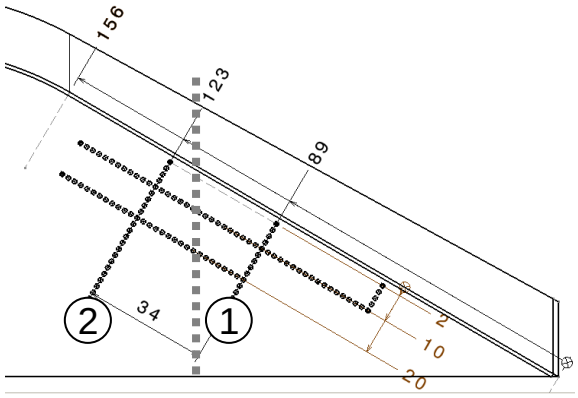

Figure 2 : Pressure holes machined in the lateral surface of the body. The dashed grey line corresponds to the location of the LDV measurement plane at x= -300 mm.

are inclined at 10° while the angle of the forward facing ramp is 30°. The junction between the ramp and the roof is rounded in order to prevent flow separation on the top of the body. Indeed, such separation would result in a strong coupling between the two A-pillar vortices. All other angles are sharp in order to control the location of flow separation. The body was carefully aligned with the oncoming flow and only a 0° angle is studied here.

The free stream velocity of this study is fixed and equal to U_∞=30 m/s. The Reynolds number based on H is then R_{eH}=1.8 10^5 and is lower than usual values for car aerodynamics. In figure 1, we see that the boundary layer is tripped at the sharp nose. The oil flow visualisation obtained by using a mixture of white spirit and kaolin powder shows that the flow remains attached on the body.

The dimensions of the exit section of the ¾ open throat anechoic wind tunnels are 450mm x 450mm. More details concerning the wind tunnel can be found in Hoarau (2006). The blockage ratio of the body plus supporting strut is 6%. The nose of the body is located at a distance of 200 mm from the exit section of the wind tunnel. Our choice was here to minimize the interactions with the ground. Therefore, the length of the streamlined supporting strut is 100 mm in order to place the body outside the boundary layer knowing that the displacement thickness of the boundary layer at that location and without any model is δ^*=1.2 mm, leading to a 99% thickness δ of order 10 mm.

The velocity measurements are obtained with a two color Laser Doppler Velocimeter (LDV) in backscatter configuration. Measurements obtained in the A-pillar vortex region will be discussed in this paper. The 0.488 µm and 0.5145 µm wavelength beams of an argon-ion laser are used to produce the LDV fringe patterns. The estimated size of the measuring volume is less than 0.1 mm in diameter and 1.3 mm long in the spanwise direction. The mean data rate is always larger than 5 kHz. The inter-arrival time weighting scheme is used to calculate the mean velocities and Reynolds stresses. A regulated glycerine smoke seeding system was specially designed for the wind tunnel and a homogeneous seeding was achieved in the measurement region. The diameter of the smoke particles is of the order of one micrometer. We have checked that they are able to track accurately the turbulent flow.

The flow will be described henceforth using a cartesian co-ordinate system (x,y,z) to indicate the axial, transverse and vertical directions. The origin is set on the symmetry plane and nose of the body (see fig. 1). The components of the instantaneous velocity field are denoted respectively by (U,V,W) where U is the longitudinal component and W is the vertical component. Only these components are measured by the present LDV system. The symbol $< >$ indicates averaging operator. The components of the instantaneous fluctuating velocity field are denoted respectively by (u,v,w). The expressions u' and w' stand respectively for longitudinal and vertical standard deviation. The number of uncorrelated events captured is always larger than 5000. Consequently, estimated statistical absolute errors for mean values are respectively $\Delta < U > \approx 0.03u'$, $\Delta u' \approx 0.02u'$ and $\Delta < uv > \approx 0.03u'v'$ with a 95% confidence level.

The measurements of the surface fluctuating pressure are obtained with off-set microphones because the distance between pressure holes can be much smaller than the one achieved with flush mounted microphones. The pressure probes are made from electret microphone cartridges connected to pressure tabs (inner diameter 0.9mm) via a pneumatic circuit (a flexible tube of length 0.3m) (Laumonier, Goudeau et al. 2001). A long tube of 2m length is connected to each sensor to adapt the impedance and to avoid acoustic resonances. For each probe, the frequency response is measured (magnitude and phase) with a B&K UA 0922 coupler and a reference microphone (see (Hoarau, Borée et al. 2006) for more details). The signal/noise ratio of the pressure probe is 50 dB. The signal recorder saves simultaneously 16 pressure signal with an effective sampling frequency of 12.8 kHz and a cut-off frequency of the anti-aliasing filters set at 6.4 kHz. The frequency response of each pressure probe is used to correct the magnitude and phase of the spectral functions. The Power Spectral Density (PSD) is estimated with the Welch's method. The time series data is split into segments of 2096 points with a 50% overlap. A Hamming window is used to compute the modified periodogram of each segment. The number of segments is 250. 16 pressure sensors are located

inside the body and all the connecting cables go through the supporting strut.

Simultaneous acquisitions along two lines perpendicular to the inclined edge of the "A-pillar" (line 1 and line 2 of figure 2) will be described in the paper. In what follows, $C_{i,j}$ corresponds to the pressure sensor number j located along line i.

3 - MEAN AND FLUCTUATING VELOCITY FIELD IN THE CONICAL VORTEX

Mean and fluctuating velocity fields were measured in a vertical plane located at x= 100 mm (100 mm from the nose of the body – see fig. 2 and 3). To be quantitative, horizontal and vertical profiles passing across the location of maximum *u'* are plotted in figures 4 and 5. This maximum is located *at* $y \approx 54mm$ and $z \approx 40mm$. The mean rotation of the conical vortex is clearly identified (consider the sign of <*W*> component in the vortex region of figure 5). A positive mean longitudinal velocity is measured in the vortex core. It is interesting to learn from fig. 5 that high values of *u'* and *w'* are detected inside the structure only (for $y \leq 61mm$).

Two maxima of *u'* and *w'* are observed on the vertical profile (fig. 4). The first one, located at z ≈ 48mm, corresponds to the 3D shear layer separating from the sharp "A-pillar". The anisotropy is large with $w'/u' \approx 1.4$. This anisotropy is believed to be associated with a vertical flapping of the shear layer. The second peak is located in the core of the vortex. Vertical fluctuations in this region are again more intense than horizontal ones ($w'/u' \approx 1.3$). We also notice in figure 4 that *u* and *w* are negatively correlated ($R_{uw} = \langle uw \rangle / u'w' \approx -0.2$ in the core and $R_{uw} \approx -0.3$ in the shear layer wrapping around the vortex core). Understanding the fluctuating character of the velocity field in such a 3D situation is a complex problem. These fluctuations are indeed the result of (i) a high turbulence level generated in the 3D swept shear layer after flow separation at the sharp edges ; (ii) an unsteady behaviour of the conical vortex itself interacting with the lateral wall of the body and (iii) a global coupling of the separated structures on the whole body.

To give a more detailed description, two points shown in figure 5 have been selected on both sides of the mean centre of the vortex. The associated pdf of *U* and *W* and a cloud of *(U,W)* points are not presented here for brevity but are discussed below. Point ❶ is located in a region of strong positive <*W*>. Nevertheless, the probability of finding negative values of *W* is non-zero and the pdf of *W* at that point is negatively skewed. On the contrary, point ❷ is located at the edge of the structure (negative value of <*W*>) but the probability of finding positive *W* is important while the pdf of *W* there is positively skewed. The signature of these extreme events is certainly due to a lateral and vertical "flapping" of the vortical structure. At point ❶, <*uw*> correlation is negative which means that high longitudinal velocities are associated (in a statistical sense) to negative

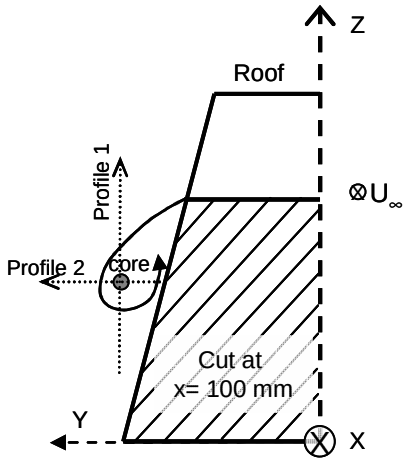

Figure 3 : Front view of the body in the LDV plane x= -300mm. Profiles shown in fig. 4 and 5.

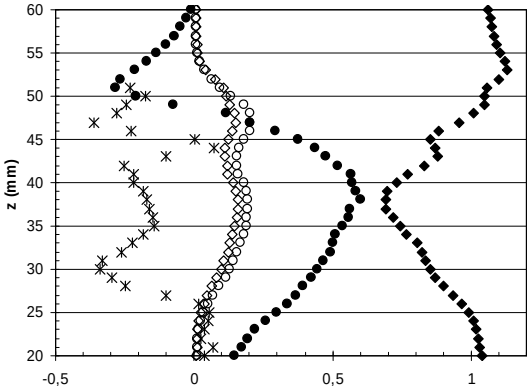

Figure 4 : Profile 1. Vertical profiles in the plane x = 100mm. The lateral location is y = 54 mm. ♦ $\langle U \rangle / U_\infty$; •, $\langle W \rangle / U_\infty$; ◊, u'/U_∞ ; ○, w'/U_∞ ; *, $\langle uw \rangle / u'w'$.

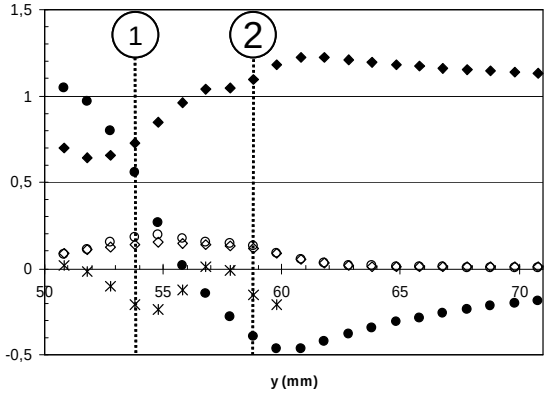

Figure 5 : Profile 2. Horizontal profiles in the plane x = 100mm. The vertical location is z = 40 mm. ♦ $\langle U \rangle / U_\infty$; •, $\langle W \rangle / U_\infty$; ◊, u'/U_∞ ; ○, w'/U_∞ ; *, $\langle uw \rangle / u'w'$.

vertical velocities. On the contrary, no significant <*uw*> correlation is measured at the mean edge of the vortex (point ❷). The signature of this velocity field on the wall pressure is now considered.

4 - SPATIO-TEMPORAL PROPERTIES OF THE FLUCTUATING PRESSURE FIELD AT THE WALL

Fluctuating pressure was measured simultaneously along the two transverse lines of figure 2. The fluctuating pressure coefficient $C_{p'}$ plotted in figure 6 was obtained by integrating the power spectral density (PSD) between 50Hz and 5kHz. The abscissa in fig. 6 is the distance ξ from the "A-pillar" sharp edge normalised by the mean reattachment distance ξ_R. The location of this mean reattachment was estimated from oil flow visualisation and can be approximated by a straight line originating from the nozzle of the body and inclined at an angle of 20°. We see that our spatial discretisation is not large enough to smoothly resolve the evolution of C_p'. The two maxima are of course detected for $\xi/\xi_R < 1$ and, beyond these maxima, the evolution of C_p' along the two lines is reasonably self-similar. The two maxima correspond respectively to the third pressure sensor of line 1 ($C_{1,3}$: $\xi = 10mm$) and to the fifth sensor of line 2 ($C_{2,5}$: $\xi = 18mm$). These two locations are first considered because it is important to study the development of the conical vortex along its axis and not "slice by slice".

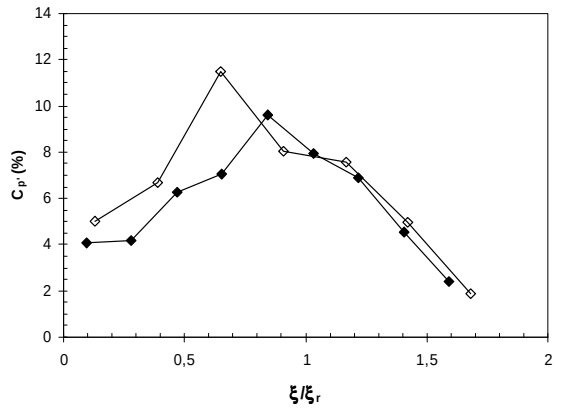

Figure 6 : Fluctuating pressure coefficient. The abscissa is the distance ξ from the "A-pillar" sharp edge normalised by the mean reattachment distance ξ_R. ◊, line 1; ♦, line 2.

The figure 7a presents both PSD at $C_{1,3}$ and $C_{2,5}$ and the modulus of the cross-spectrum. The figure 7b shows the coherence of both signals while the figure 7c shows the phase evolution in a frequency domain restricted to the domain where the coherence is larger than 0.1. At $C_{1,3}$, the PSD is maximum in the frequency band $f \in [2kHz, 3kHz]$. This maximum shifts toward lower frequencies on the second transverse line and corresponds approximately to the frequency interval $f \in [1.5kHz, 2.5kHz]$ at $C_{2,5}$. One interesting result is that the values of the cross-spectrum and of the coherence are very weak in these frequency bands. The physical phenomena responsible for these maxima are therefore only weakly correlated.

On the contrary, we observe a very clear local maximum of both PSD, of the cross-spectrum and of the coherence centred at *f≈1 kHz*. Moreover, even if the energy content is lower, the coherence between both signals is high in the low frequency region (very large peak centred at *f≈300 Hz*). In figure 7c, we measure a quasi-linear evolution of the phase angle with frequency. Indeed, the slight rupture is only measured in the region where the coherence is weak.

Cross spectra between $C_{1,3}$ and all sensors of line 1 and $C_{2,5}$ and all sensors of line 2 were also computed. The interaction energy can be integrated in the three distinct frequency bands $[200Hz, 700Hz]$, $[700Hz, 1.5kHz]$ and $[1.5kHz, 4kHz]$. If this interaction energy is normalised by the local total interaction energy, we observe that the "high frequency" contribution is dominant only in the neighbourhood of the reference sensor. On the contrary, the local relative contributions in the two lower frequency bands are approximately constant across the vortex structure and even beyond the mean reattachment point. This shows that the corresponding physical events have a large scale transverse coherent signature.

5 - DISCUSSION

In 2D separated flows, the link between the velocity field and the fluctuating wall pressure field is clearly established. In particular, large scale structures shedded from separated region are transported downstream and dissipate over the recovering boundary layer (Castro and Epik 1998) and their wall pressure signature is very clear (Hoarau et al. 2006). These results are difficult to extend to fully 3D aerodynamical situations. However, we are here in a particular situation in which the wall pressure fluctuations are associated to perturbations of the conical vortex structure itself or to smaller scale perturbations transported by this particular flow structure. Let's conjecture here that the eduction of the flow velocity field projected along the direction of the vortex core is important in this particular region of the flow field. We locate approximately the centre of the vortex at the point of maximum turbulence in the plane $x = 100mm$: (y,z)=(54mm,40mm). A straight line drawn from the corner of the nozzle of the body and passing through this point has then an angle of θ ≈22° with the x-axis in a vertical plane and a small angle of φ≈3° with the x-axis in a horizontal plane. Neglecting φ, we can easily obtain from the two-component LDV measurements, the two components U_a and W_a of the velocity field respectively aligned with the vortex axis and perpendicular to it in a vertical plane containing the axis. U_a and W_a read $U_a = U\cos\theta + W\sin\theta$ and $W_a = -U\sin\theta + W\cos\theta$. Mean and rms quantities are then computed and the horizontal profiles presented in figure 8 are associated with the data displayed in figure 5. The mean rotation is clearly detected in fig. 8 and we now see that the maximum of the rms values are located at $\langle W_a \rangle \approx 0$. Moreover, the correlation coefficient $R_{u_a w_a} = \langle u_a w_a \rangle / u_a' w_a'$ is very small.

Noticeably, the axial mean velocity $\langle U_a \rangle$ is quasi-constant across the core of the vortex with $\langle U_a \rangle \approx 28\,m/s$.

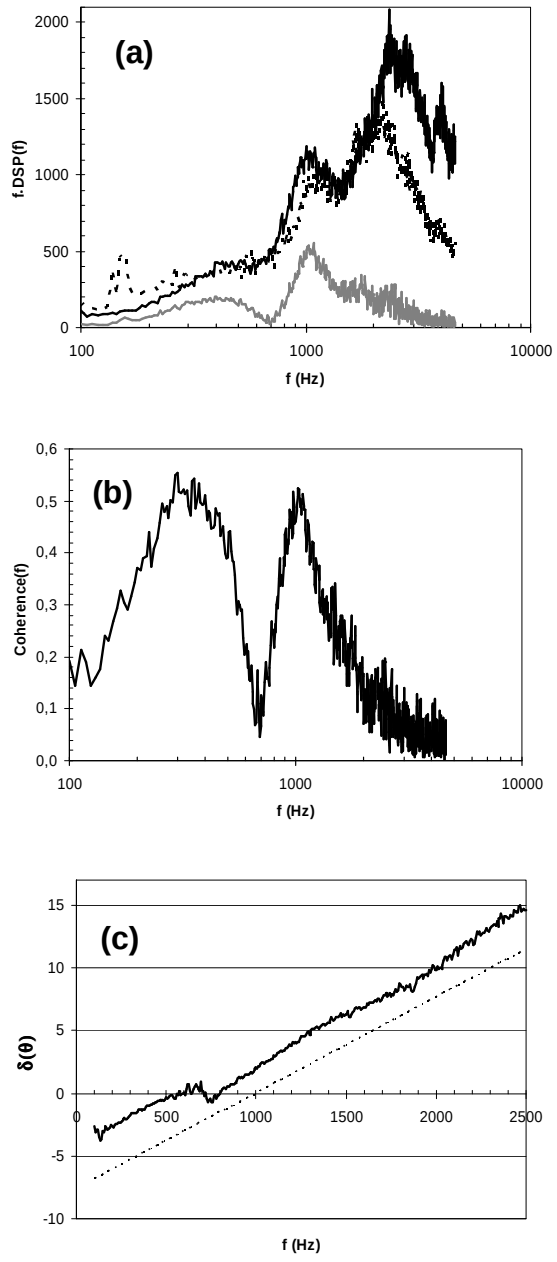

Figure 7 : a, Power spectral densities at $C_{1,3}$ (——) and $C_{2,5}$ (– –) and modulus of the cross-spectrum (——) ; b, Coherence of both signals; c, Phase evolution in the frequency domain restricted to the domain where the coherence is larger than 0.1. The dashed straight line in figure 7c is introduced and discussed in part 5.

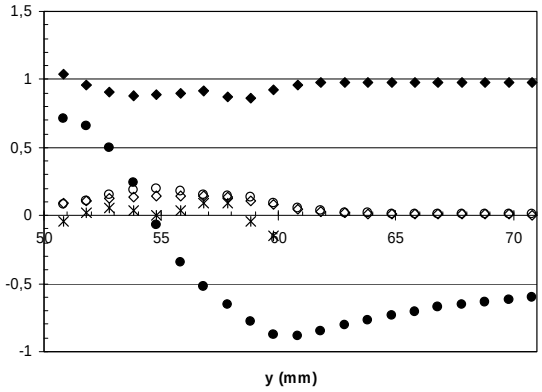

Figure 8 : Horizontal profiles of the components of the velocity field in a local referential aligned with the vortex axis. Profile in the plane x= -300mm. The vertical location is z=-50 mm. ♦ $\langle U_a \rangle / U_\infty$; •, $\langle W_a \rangle / U_\infty$; ◊, u_a'/U_∞ ; ○, w_a'/U_∞ ; *, $\langle u_a w_a \rangle / u_a' w_a'$.

Considering again the wall pressure fluctuations discussed previously (figures 7a,b and c), we observe that, for perturbations transported by the velocity field at a constant mean velocity U_C, the slope of the phase evolution is simply $d(\delta\theta)/df = 2\pi \Delta L / U_C$. Such elementary relation seems difficult to apply to a 3D velocity field. However, we are here in a particular situation with a quasi-uniform mean velocity component when the velocity is projected in the direction of the axis of the conical vortex (fig. 8). The slope of the straight line drawn in figure 7c has thus been computed by assuming that perturbations are transported along the core of the vortex at the velocity $U_C = \langle U_a \rangle \approx 28\,m/s$ and by using the distance ΔL=34mm between both pressure sensors. A very good agreement is observed and shows that the perturbations are guided and transported along the axis of the conical vortex at the mean axial velocity.

Representative length scales can be associated to both peaks of coherence observed in figure 7b. For the low frequencies, $f.L_1/U_C \approx 1$ with $U_C \approx 28\,m/s$ and $f \approx 300Hz$ leads to $L_1 \approx 90mm$. The associated length scale is thus of the order of the full length of the conical structure and we might associate this contribution to a meandering of the structure. At intermediate frequencies, $f.L_2/U_C \approx 1$ with $U_C \approx 28\,m/s$ and $f \approx 1kHz$ leads to $L_2 \approx 28mm$. L_2 is of the order of the transversal size of the structure and might be associated with perturbations generated during the rolling-up of the unsteady vorticity sheet (a 3D equivalent to vortex shedding) transported along the core of the vortex, the conical vortex being here a guide for these large scale perturbations in a 3D situation. Finally, let's consider the energy containing higher frequency part of the PSD. Signals associated to sensors $C_{1,3}$ and $C_{2,5}$ are only weakly correlated in this frequency band. We therefore conjecture that this contribution is due to a 3D turbulent field generated in the shear layers and uncorrelated between $C_{1,3}$ and $C_{2,5}$ because it's turn over time scale is too short.

One more hint supporting this hypothesis comes from the shift toward lower frequencies detected when comparing both PSD (fig. 7a). If we suppose that these physical events are associated to a similar Strouhal number scaling on the local reattachment length ξ_R, we should get $f_1\xi_{R1}/U_\infty \approx f_2\xi_{R2}/U_\infty \Rightarrow f_2/f_1 \approx \xi_{R1}/\xi_{R2}$. With $f_2 \approx 2.5kHz$ and $f_1 \approx 2kHz$, one gets $f_2/f_1 \approx 0.8$ while $\xi_{R1}/\xi_{R2} \approx [89tg(20)/123tg(20)] \approx 0.72$ (see fig. 2). The frequency shift is therefore expected to be due to the contribution of a turbulent field adapting itself to the development of the conical vortex.

6 - CONCLUSION

The spatio-temporal properties of the unsteady wall pressure field of a model A-pillar conical vortex was studied in this paper by combining 2 components LDV measurements and multi-points pressure measurements using off-set microphones. The model body has sharp edges. Detailed LDV measurements have been displayed in the vortex region. A conical vortex develops along the side walls of the body. Both the 3D shear layer separating from the sharp edges and the vortex core are highly fluctuating regions. Moreover, the magnitude of vertical rms velocities is significantly larger than the axial rms velocities ($w'/u' \approx 1.3$). These fluctuating velocities are the signature of both an unsteady behaviour of the organised vortical structure interacting with the wall and of finer scale turbulence carried by the unsteady flow. We show that the spectral analysis – PSD, cross spectrum, coherence – of the fluctuating pressure at distant pressure sensors located near the line of maximal Cp' – that is to say under the vortex core – is useful to analyse the link between the temporal and spatial scales of the unsteady aerodynamic and the wall pressure field. In particular, we have shown that the conical vortex is a guide for the velocity perturbations and that their hydrodynamic pressure footprint is transported at the measured mean axial velocity in a local reference frame aligned with the vortex core. Two distinct peaks of coherence can then be associated with perturbations having (i) a length scale of the order of the full length of the conical structure ; (ii) a length scale of the order of the transversal size of the structure. These perturbations may correspond to a global meandering of the structure (Low frequency contribution) and to large scale perturbations generated during the rolling-up of the unsteady vorticity sheet. Noticeably, the energy containing higher frequency parts of the PSD are only weakly correlated when distant sensors are considered. We show that the associated physical events correspond to a similar Strouhal number scaling on the local reattachment length. We therefore conjecture that they correspond to the contribution of a turbulent field adapting itself to the development of the conical vortex and uncorrelated between distant sensors because it's length scale and turn over time scale is too short.

The three distinct contributions extracted here from the combined study of the pressure and velocity fields have a significant impact as Cp' is concerned and might be transmitted in very different ways by the car structure because the frequency and length scale range is very distinct. Energy transfer and non-linear interactions between these components are of course expected and were not studied here. This is a necessary step for a good understanding and eventually for the control of this unsteady aerodynamic.

Aknowledgements

The set-up was built in the context of a National Research group CNRT *"Recherche en Aérodynamique et Aéroacoustique pour les véhicules terrestres"* supported by Renault SA and PSA Peugeot-Citroen. C. Hoarau thanks the CNRT for financial support.

The technical support of P. Braud and L. Philippon is greatly acknowledged. We thank the staff of the LEA mechanical workshop.

REFERENCES

Alam, F., S. Watkins and G. Zimmer (2003). "Mean and time-varying flow measurements on the surface of a family of idealised road vehicles." Experimental Thermal and Fluid science **27**: 639-654.

Castro, I. P. and E. Epik (1998). "Boundary layer development after a separated region." J. Fluid Mech. **374**: 91-116.

Delery, J. (1994). "Aspects of vortex breakdown." Progress in Aerospace Sciences **30, n°1**: 1-59.

Hoarau, C. (2006). Mesures multipoints pression-vitesse pour l'analyse de l'aérodynamique d'écoulements décollés instationnaires. Application aux véhicules terrestres., PhD Thesis - University of Poitiers.

Hoarau, C., J. Borée, J. Laumonier and Y. Gervais (2006). "Analysis of the wall pressure trace downstream of a separated region using extended proper orthogonal decomposition." Physics of fluids **18, (5)**.

Kawai, H. and G. Nishimura (1996). "Characteristics of fluctuating suction and conical vortices on a flat roof in oblique flow." J. Wind Eng. Ind. Aerodyn. **71**: 579-588.

Laumonier, J., C. Goudeau and Y. Gervais (2001). Mesures aérodynamiques sur profil NACA 0012 avec décollement. 2001. Colloque " Bruit des ventilateurs à basse vitesse ", Ecole Centrale de Lyon, Novembre.

Lehugeur, B. and P. Gillieron (2006). Drag reduction by active control of A-pillar vortex breakdown on a simplified car geometry. European Drag Reduction and Flow Control Meeting. 10-14th April, Ischia, Italy.